

Firing of hippocampal neurogliaform cells induces suppression of synaptic inhibition.

Gengyu Li, Robert Stewart, Marco Canepari, Marco Capogna

▶ **To cite this version:**

Gengyu Li, Robert Stewart, Marco Canepari, Marco Capogna. Firing of hippocampal neurogliaform cells induces suppression of synaptic inhibition.. Journal of Neuroscience, 2014, 34 (4), pp.1280-92. 10.1523/JNEUROSCI.3046-13.2014 . inserm-00951405

HAL Id: inserm-00951405

https://inserm.hal.science/inserm-00951405

Submitted on 4 Jun 2014

HAL is a multi-disciplinary open access archive for the deposit and dissemination of scientific research documents, whether they are published or not. The documents may come from teaching and research institutions in France or abroad, or from public or private research centers.

L'archive ouverte pluridisciplinaire **HAL**, est destinée au dépôt et à la diffusion de documents scientifiques de niveau recherche, publiés ou non, émanant des établissements d'enseignement et de recherche français ou étrangers, des laboratoires publics ou privés.

Firing of hippocampal neurogliaform cells induces suppression of synaptic inhibition

Gengyu Li[1], Robert Stewart[1], Marco Canepari[2, 3, 4] and Marco Capogna[1]

[1]MRC Anatomical Neuropharmacology Unit, Department of Pharmacology, University of Oxford, United Kingdom; [2] Inserm U836, Team 3, Grenoble Cedex 09, France

[3] Université Joseph Fourier, Grenoble Institut des Neurosciences and Laboratoire Interdisciplinare de Physique (CNRS UMR 5588), France

[4] Laboratories of Excellence, Ion Channel Science and Therapeutics

Corresponding Author: Dr. Marco Capogna, MRC Anatomical Neuropharmacology Unit, Mansfield Road, Oxford, OX1 3TH, UK. marco.capogna@pharm.ox.ac.uk

Number of figures and tables: 9and 0

Number of pages: 40

Number of words for Abstract (200), Introduction (500), and Discussion (1432)

Acknowledgements: This work was supported by the Medical Research Council, UK (MRC award U138197106). We thank Katherine Whitworth for preparing the solutions and help with re-sectioning slices, andtogether with Liz Norman for generating and breeding the nNOS-Cre-tdTomatomice, Dr. Jeremy Graham (Cairn Research Ltd., Faversham, UK) for help to set up the laser-illumination system to detect voltage sensitive dye signals. Prof. Thomas Klausberger &Prof. Peter Somogyi are acknowledged for the use of firing patterns recorded *in vivo* in hippocampal NGFCs.Dr. Michael Bazelot and Marco Bocchio (MRC ANU) are acknowledged for their comments on the manuscript.

Abstract

Little is known on how neuron firing recorded *in vivo*retrogradely influences synaptic strength. We injected the firing of arat hippocampal neurogliaform cell (NGFC), a widely expressed GABAergic neuron type, detected *in vivo* during theta rhythm, into a rat NGFCrecorded*in vitro*. We found that the "*in vivo* firing pattern" produced a transient firing-induced suppression of synaptic inhibition (FSI) evoked by a presynaptic NGFC. Imaging experiments demonstrate that FSI was correlated to action potential backpropagation (bAP) and a supralinear increase in dendritic Ca^{2+}. The application of the L-type Ca^{2}+ channel antagonist nimodipineblocked FSI. Further pharmacological experiments, such as theapplication of a nitric oxide-sensitive guanylylcyclase (NO-sGC) receptor antagonist, a NOS inhibitor and NO donors,as well as the use of nNOS-Cre-tdTomatomicesuggested that NO released from postsynaptic cellsmediated FSI and likely activated presynaptic receptors to inhibit GABA release. The "*in vivo* firing pattern" modulated the size of unitary EPSPs impinging on NGFCs through FSI and not via a direct effect on excitatory synaptic transmission. Our data demonstrate: 1) retrograde signaling initiated by "*in vivo* firing pattern", 2) interneuron bAPsdetected with fast time resolution, and 3) a novel role for NO expressed by specific interneuron types.

Introduction

Various GABAergiccellscontain different Ca^{2+}-binding proteins (e.g. calbindin, calretinin and parvalbumin) or peptides (e.g. cholecystokinin, somatostatin and substance P)(Klausberger and Somogyi, 2008). The cell-specific presence of such cell markersis often used for a neurochemical classification of interneuron diversity(Maccaferri and Lacaille, 2003). For example, the specific expression of calbindin,calretininandparvalbuminidentifies groups of interneurons with different geometry of dendritic architecture, postsynaptic target specificity and synaptic input density (Gulyas et al., 1999). Moreover, neurochemical markers are usedtoscrutinize the selective susceptibility of specific interneurons to pathological conditions, such as epilepsy (Cossart et al., 2001)and ischemia(Freund et al., 1992). In contrast to the neurochemical data, information on the physiological role of interneuron markers is scant, albeit there are some exceptions. For example, parvalbumin (PV), which labels various types of interneurons(Klausberger and Somogyi, 2008)and is a slow Ca^{2+} buffer(Baimbridge et al., 1992),contributes to short-term synaptic depression evoked by PV expressing interneurons, andis likely to prevent the harmful effects of excessive Ca^{2+} accumulation in pathological conditions(Caillard et al., 2000). The neuropeptide Y, which is also expressed by several interneuron types(Karagiannis et al., 2009), is likely to be an endogenous anti-epileptic peptide in the hippocampus (Colmers et al., 1991).

The interneurons of the hippocampus that expressthe neuronal nitric oxide synthase (nNOS) are very abundant (Fuentealba et al., 2008). ThenNOS expressing neurons comprise some CA1 pyramidal neurons and several types of interneurons including: neurogliaform cells (NGFCs)(Price et al., 2005), ivy cells (Fuentealba et al., 2008), interneuron-specific interneurons co-expressing thevasoactive intestinal peptide and calretinin, a subset of PV expressing interneurons of the dentate gyrus, a subset of

somatostatin expressinginterneurons, and projection cells with the soma close to the subiculum(Tricoire and Vitalis, 2012). Despite their wide distribution, the functional role of NO in nNOS-expressing hippocampal interneurons is not known. In the neocortex, the NO released by NGFCs has been proposed to regulateneurovascular coupling and blood flow(Cauli et al., 2004).

To study the physiological roleof nNOS expressing interneurons of the hippocampus, we capitalized on a database of firing patterns of anatomically-identified hippocampal interneurons recorded *in vivo*(Klausberger and Somogyi, 2008). We injected the firing of anNGFC detected *in vivo* during theta rhythm (Fuentealba et al., 2010), into NGFCsrecorded*in vitro*. We chose NGFCs because a good proportion of them expresses nNOS, they are frequentlysynaptically-coupled, they display few and short dendrites well preserved *in vitro* and they are biophysically compact (Vida et al., 1998; Price et al., 2005; Tricoire et al., 2010). These features make theman excellent cell type to study NO-dependent signaling by using unitary synaptic transmission and dendritic imaging. We found that the NGFC *in vivo*firing pattern elicited a depolarization-induced suppression of inhibition (DSI)-like phenomenon(Llano et al., 1991; Pitler and Alger, 1992).We termed this phenomenon firing induced suppression of inhibition (FSI). We report here the mechanisms, the signaling and the role of FSI on NGFCsynaptic integration.

Materials and Methods

Slice preparation

All procedures involving animals were performed using methods approved by the United Kingdom Home Office and according to The Animals (Scientific Procedures) Act (1986). Juvenile male and female rats (P15 – P22) or neuronal nitric oxide synthase

(nNOS)-Cre-tdTomatomale and female mice (P29 – P40) were anesthetised with isoflurane and decapitated. The brain was carefully removed and mounted on the plate of a vibratome(Microm HM 650 V, Thermo Fisher Scientific Inc., Germany)in ice-cold ACSF containing (in millimolar, mM): 85 NaCl, 25 $NaHCO_3$, 2.5 KCl, 1.25 NaH_2PO_4, 0.5 $CaCl_2$, 7 $MgCl_2$, 10 glucose, 75 sucrose saturated with 95% O_2 and 5% CO_2, at pH ~7.3. Horizontal sections (thickness: 325 µm) consisting of the dorsal hippocampus and attached entorhinal cortex were prepared using a vibratome. During the initial period of slice storage (~ 20 min), the cutting solution was replaced with normal ACSF (containing in mM: 130 NaCl, 24 NaHCO3, 3.5 KCl, 1.25 NaH2PO4, 2.5 CaCl2, 1.5 MgSO4, 10 glucose saturated with 95% O2, 5% CO2, at pH 7.3). Slices were then maintained at room temperature (18-22˚C).

Acute slices were then placed in a recording chamber mounted on the stage of an upright microscope (Olympus BX 51WI or Axioscope, Zeiss) equipped with immersion differential interference contrast objectives (40x, 60x) coupled to an infrared camera system (Hamamatsu, Hamamatsu City, Japan), superfused at a rate of ~2 ml/min with oxygenated recording ACSF and maintained at a temperature of 33 ± 1 ºC.

Electrophysiology recordings and analysis

Whole-cell recordings were performed using EPC10/3 or EPC9/2 amplifiers (HEKA, Lambrecht, Germany). Rat interneurons with the soma in the stratum lacunosummoleculare(SLM) were identified based on soma shape and size under infra-red video microscopy. Mouse interneurons with the soma in the SLMexpressing tdTomato under fluorescence illumination were selectively recorded. Borosilicate patch pipettes were pulled (Zeitz puller – DMZ, Martinsried, Germany), and filled with a solution containing (mM): 88 KCl, 42 K-gluconate, 10 HEPES, 10 Na2Phosphocreatine,

4 Mg-ATP, 0.3 Na-GTP, pH 7.3 with KOH, in order to increase the driving force for Cl- ions (ECl = -11 mV) to the extent that the IPSC polarity was inward at the holding potential (Vh) of -65 mV. In dynamic clamp experiments performed in current clamp mode, the intracellular solution contained (mM): 126 K-gluconate, 10 HEPES, 10 Na_2Phosphocreatine, 4 KCl, 4 Mg-ATP, 0.3 Na-GTP, pH 7.3 with KOH, the osmolarity was 270-280 mOsmol. Biocytin was added to the intracellular solutions before recording at a final concentration of 2-4 mg/ml. Pipettes had resistances of 5-6 MΩ when filled with the internal solution containing 88 mMKCl. Access resistance was always monitored to ensure the stability of recording conditions. Cells were only accepted for analysis if the initial series resistance was less than or equal to 20 MΩ and did not change by more than 20% throughout the recording period. No correction was made for the junction potential between the pipette and the ACSF, and therefore the recorded membrane potential, as calculated post-hoc using a junction potential calculator, was 16 mV and 11 mV more depolarised than the true membrane potential, for K-gluconate and high-Cl^- intracellular solution, respectively.

Action currents or potentials were elicited in a presynaptic cell by using a short depolarising voltage step (from the holding potential of -68 mV to 0 ms, 3 ms) or a short depolarizing current step (500-1000 pA x 3 ms, from –68 mV). The corresponding unitary inhibitory postsynaptic current (uIPSC) or unitary inhibitory postsynaptic potential (uIPSP) was recorded in a synaptically-coupled postsynaptic neuron or in the presynaptic neuron as an autaptic IPSC (aIPSC). Postsynaptic and autaptic currents were filtered at 3 kHz and recorded with a sampling rate of 5 kHz. Spontaneous inhibitory postsynaptic currents (sIPSCs) were also recorded at Vh = -65 mV filtered at 3 kHz with a sampling rate of 10 kHz for 120 s.

The *in vivo*firing sequence was recorded in an identified NGFC in an

anesthetised rat with the juxtacellular/extracellular method during theta oscillations and previously published (Fuentealba et al., 2010). This firing sequencelasting 60 s wastransformed as voltage pulses (100 mV, 1 ms each) using MATLAB (The MathWorks Inc., Natick, MA, USA) software, and injected as stimulus protocol to induce FSI into whole cell patch clamped cells usingPatchMaster (Heka) software. The stimuli evoked a train of action potentials *in vitro* that exactly matched the sequence of action potentials detected *in vivo*. A recorded pair was classified as having FSI if the uIPSC or uIPSP evoked 125 to250 ms after the end of the stimulation protocol applied to the postsynaptic cell was decreased>5% followed by full recovery of the peak amplitude of the response. In the majority of the cases the stimulation protocol was repeated several times (typically 3 times) for each experiment followed by at least 2 stimulations with recovery.

Electrophysiological data were analyzed offline using custom made MATLAB software.For FSI analysis, FSI amplitude was measured as $1 - \frac{IPSC(P)_{FSI}}{IPSC(P)_{control}}$, where $IPSC(P)_{FSI}$ is the amplitude of IPSC(P) 125 or 250 ms after the stimulus protocol, and $IPSC(P)_{control}$ is the average amplitude of three IPSC(P)s acquired before conditional protocol. For kinetics analysis, the 20% - 80% rise time and decay time constant (τ_{syn}) were calculated by fitting a single exponential in the form of $Ae^{bx} + C$ in each trace. The decay of the uIPSCs could also be fitted with a double exponential, and the weighted decay time constant was calculated using the following formula: $\tau_w = \tau_1 A_1 + \tau_2 (1- A_1)$, where τ_w is the weighted decay time constant, τ_1 and τ_2 are the time constants of the first and second exponential functions, respectively, and A_1 is the proportion of the peak amplitude of the averaged uIPSC that is contributed by τ_1.For passive and active electrophysiological property analysis: the input resistance (R_{in}) was calculated as the inverse of the gradient of the linear fit from an I/V plot of the recorded cell (current

injectedagainst steady state voltage response); membrane time constant (τ_{mem}) was calculated by fitting a single exponential $(Ae^{bx} + C)$; membrane capacitance was calculated as τ_{mem}/R_{in}; the sag rectification ratio was calculated from the membrane potential at the end of 500 ms hyperpolarizing divided by the largest membrane potential change observed in response to a current step of -200 pA; and the adaptation index wasdefined as the interspike interval between the last versus the first action potential evoked by a depolarizing current pulse lasting 500 ms.The peak amplitude and half-widthwere measured from the initial point of the rising phase of theaction potential.The coefficient of variation (CV) for the stimulation protocol was calculated as the standard deviation of interspike intervals/mean of interspike intervals.

Synthetic (dynamic clamp) EPSPs (dEPSPs) were applied through the patch pipette using a synaptic module (SM-1) conductance injection amplifier (Cambridge Conductance, Cambridge, UK). The dynamic conductance waveform for an EPSP was based on the magnitude, kinetics and reversal potential of the EPSC experimentally evoked by minimal stimulation in the same cell in voltage clamp prior to the dynamic clamp experiment (dEPSPpeak conductance = 0.5 - 2nS, 20-80% rise time = 0.6 – 0.7ms, decay τ= 3– 4ms, reversal potential set at 0 mV).dEPSP data was analyzed with scripts written in MATLAB. Ten dEPSPs were applied at 80 Hz and the peak amplitude of eachdEPSPwascalculatedfrom its baseline before,during andafter FSI. To obtain dEPSPs, minimal extracellular stimulation was conducted by applying rectangular pulses of current (0.4 ms width, intensity range: 10-15 μA) delivered through an isolation unit (A360 Stimulus Isolator, World Precision Instruments, Stevenage, UK) to a monopolar patch pipette filled with ACSF placed closed to the recorded cell (5 μM gabazine and 50μM CGP35348 added to extracellular ACSF).

Paired or un-paired Student's t-tests, where appropriate, were performed with SPSS (Surrey, UK) or Prism 4.0 (Graphpad Software, La Jolla, Ca, USA). When other statistical tests have been used then they have been specified in the text. Statistical significance was set at $p < 0.05$. Values presented in the text and in figures represent the mean ± SEM unless otherwise stated.

Voltage sensitive dye and calcium imaging recordings and analysis

In voltage sensitive dye (VSD) and Ca^{2+} imaging experiments, a low chloride internal solution containing (in mM): 140 K-gluconate, 10 HEPES, 10 Na_2Phosphocreatine, 4 Mg-ATP, 0.3 Na-GTP, pH 7.3 with KOH was used. The VSD JPW1114 (0.25-0.5mg/ml) was loaded into the cell by using the whole cell patch clamp recording of the cell soma described in detail previously(Canepari et al., 2008). Briefly, the whole-cell configuration used for dye loading lasted 30–40 minutes and then the patch pipette was removed from the cell by forming an outside-out patch. The cell was then incubated for additional 60–90 minutes to allow dye equilibration into dendrites and re-patched with a dye-free pipette containing biocytin (2-4mg/ml). Voltage fluorescence was excited with a 532 nm-300 mW solid state laser (model MLL532; CNI, Changchun, China) as described previously(Canepari et al., 2010). In Ca^{2+} imaging experiments, the low-affinity indicators Oregon green 5N (OG5N) or Mag-Fura-2 (MF2) were added at 0.5 mM concentration to the internal solution. Ca^{2+} fluorescence was excited with an OptoFlash (Cairn Research Ltd., Faversham, UK) using either a 470 nm LED (for OG5N) or a 385 nm LED (for MF2), mounted on the epifluorescence port of the microscope. The excitation light, either from the laser or the LED, was directed to a water immersion objective (Olympus 60x/1.1 NA). Fluorescent images, de-magnified by 0.25x or 0.38x, were visualised with a high speed CCD camera NeuroCCD-SM

(RedShirtImaging LLC, Decatur, GA, USA) at a frame rate ranging between 125 Hz and 5 kHz. The corresponding electrophysiological signals from the soma were recorded at a frequency ranging between 8 kHz and 20 kHz. The CCD has 80X80 pixels covering an area of 125µmX125µm with the 0.25X de-magnifier and 82µmX82µm with the 38X de-magnifier. The area covered by a single pixel was 1.6µmX1.6µm and 1µmX1µm with the 0.25X and 0.38 de-magnifiers respectively. The dendritic regions analysed in this study were within 20-120µm from the soma.

Both VSD and Ca^{2+} imaging data were analysed with dedicated software written in MATLAB. Optical signals were initially expressed as fractional changes of fluorescence averaged from 4x4 (16 pixels) regions of interest (ROIs) and obtained from averages of four trials unless otherwise mentioned. The fractional change of fluorescence was computed as the change of fluorescence of each individual frame from the initial fluorescence divided by the initial fluorescence. A bleaching sweep (without signal) was acquired and subtracted to the signal sweeps.For calibration of VSD signals, a "reference" signal associated with a long lasting hyperpolarizing current pulse (-50/-100pA, 350 ms) was injected into the soma and recorded (400 ms x 9-16 sweeps) at low acquisition rate (typically 125 frames/s) using a moderate illumination (usually 3mW) to minimize bleaching and photo-toxicity. This signal should spread with minimal attenuation along the dendrites (Vetter *et al.*, 2001) providing a uniform membrane potential change along the dendrite. Thus, because the VSD ΔF/F signal is linear with the membrane potential change, any ΔF/F can be converted into mV using the same procedure described elsewhere(Canepari and Vogt, 2008)for cerebellar Purkinje neurons.The amplitude of the images resulted from the average value DF/F during steady state pulse subtracted (usually 50 ms) from DF/F value immediately before the onset of the pulse, baseline 10-20 ms DF/F mean value.

To calibrate fractional changes of OG5N fluorescence into changes of intracellular free Ca^{2+} ($\Delta[Ca^{2+}]$free), we used the low-affinity indicator MF2 (Kd = 25µM). When excited at 385 nm, this indicator exhibits a decrease in fluorescence associated with an increase in Ca^{2+} and the $\Delta[Ca^{2+}]$free can be estimated as Kd•(Fmin-F)/(F-Fmax), where Fmin and Fmax are the fluorescence at 0 and saturating Ca^{2+} respectively. This indicator has an excellent dynamic range and in Cueni et al. (2008) we have shown that at high concentrations (>0.5 mM), Fmin and Fmax can be approximated with the initial fluorescence and the slice autofluorescence respectively. In addition MF2 fluorescence is not excited at 470 nm, i.e. at the excitation wavelength of OG5N. Thus, in a series of calibraton experiments, we added the two indicators together at 0.5 mM concentration in the patch pipette and monitored fluorescence signals associated with one to four action potentials to calibrate the OG5N fractional change of fluorescence into $\Delta[Ca^{2+}]$free.

Intracellular Labelling and post-hoc Visualisation of Recorded Cells

After recordings, the slices were immersed at 4° C for 12-24hrs in a fixative solution containing: 4% paraformaldehyde, 15% (v/v) saturated picric acid and 0.1 M phosphate buffer (PB; pH 7.2-7.4). Then, gelatine-embedded slices were re-sectioned into 60 µm thick sections. Sectionswere then incubated with streptavidin-Cy3 solution (93% of 0.1 M phosphate buffer, 6% of Triton at 3% and 1% of Streptavidin-Cy3) or Alexa-Fluor 350-conjugated streptavidinovernight before mounting and imaging them under a fluorescent microscope. Pictures of the location and the dendritic/axonal patterns of the recorded neurons were performed and stored. After this step, some sections were further processed to reveal the fine details of the processes of the cells using the diaminobenzidine (DAB) staining method. In brief, sections containing

biocytin-filled cells were incubated in avidin-biotinylated horseradish peroxidase complex (1:100 dilution; ABC Kit; Vector Laboratories, Burlingame, CA) followed by a peroxidase reaction using diaminobenzidine (DAB, Sigma-Aldrich; 0.05%) as the chromogen and 1% H_2O_2 as the substrate. Sections were then mounted on gelatine-coated slides, air-dried, immersed in xylene-based mounting medium (Entellan; Merck, Damstadt, Germany) and cover-slipped.

The nNOS-Cre-tdTomatomouse line was generated using methods described previously(Taniguchi et al., 2011). Tamoxifen administration was used to induce Cre activity in nNOS expressing neurons. Tamoxifen was administrated by intraperitoneal injection at 2-5 mg/dosage three times every other day from P21. When immunohistochemistry was performed on sections of nNOS-Cre-tdTomatomice, re-sectioned slices (50 μM) were incubated with a primary antibody raised against nNOS (1:500 goat ab1376, Abcam) and tdTomato (1:500 Rat RFP 5F8, Chromotek) overnight at 4° C in 0.3% Triton X-100 and 10% normal donkey serum containing PBS-azide buffer. The nNOS staining was revealed using AlexaFluor488-conjugated secondary antibody (1:500 donkey to goat, Invitrogen), and tdTomato staining was revealed using Cy3-conjugated secondary antibody (1:1000 donkey to rat, Jackson Immunoresearch).

For cell counting experiments, re-sectioned slices of nNOS-Cre-tdTomatomice were visualised under a confocal microscope (Zeiss LSM 710). Images were acquired using the acquire SRS image stack workflow function in StereoInvestigator (MBF Bioscience), in which the whole hippocampus was included. Cell counting (interneurons and pyramidal cells) was carried out offline: the digital copy of each section was opened in StereoInvestigator, the guard zone was 2μm and the probe length was 10 μm, only cells with soma in the probe zone were counted.

Chemicals and drugs

All drugs were applied to the recording preparation through the bath. Salts used in the preparation of the intracellular recording solution and ACSF were obtained from either BDH Laboratory Supplies or Sigma (Poole, UK). Kynurenic acid, biocytinwas purchased from Sigma (Poole, UK), 6-Imino-3-(4-methoxyphenyl)-1(6H)-p-yridazinebutanoic acid hydrobromide (SR95531), CGP35348, 1H-[1,2,4]Oxadiazolo[4,3-a]quinoxal-in-1-one (ODQ), NG-Nitro-L-arginine methyl ester hydrochloride (L-NAME), L-arginine,nimodipine, ryanodine, U73122 were purchased from Tocris Cookson (Bristol, UK).

Results

In vivo firing induces a transient suppression of synaptic inhibition

Unitary inhibitory postsynaptic potentials (uIPSPs) or currents (uIPSCs) were recorded from synaptically-coupledputative NGFCsin the SLM of rat hippocampus *in vitro*. Due to high $[Cl^-]_i$these events were depolarizingpotentials (current clamprecordings at -68 ± 2 mV) or inward currents (voltage clamprecordings at -68 ± 2 mV). A firing sequence (60 s duration, average frequency and CV values: 8.3 Hz, 0.75;stimulation protocol) recorded in a rat NGFC *in vivo*during theta oscillations (Fuentealba et al., 2010)was injected in current clamp mode in a postsynaptic interneuronof the SLM recorded *in vitro*. This caused a transient decrease in the amplitude of the uIPSPsrecorded in current clamp occurring shortlyafter (125 or 250ms) the *in vivo* firing injection (75 ± 1.4% of control, $p < 0.001$) in 23/70cell pairs tested (Figure 1A, C). Likewise, the stimulation firing elicited a transient decrease in the amplitude of the uIPSCsrecorded in voltage clamp (71.7 ± 2.6% of control, $p < 0.001$) in 11/26 cell pairs tested (Figure 1B, C). The

kinetics of control and decreased uIPSCsevoked before and immediately after the stimulation protocol was similar (Figure 1B, inset) (rise-time was 97 ± 4% of control, $p > 0.1$; weighted decay time constant was 98 ± 12% of control, $p > 0.1$, $n = 9$), suggesting that presynaptic mechanismswere more likely than postsynaptic ones to underlie the decrease of the synaptic responses.Sixty seconds after the end of the stimulationprotocol the uIPSPs or uIPSCs returned to control level and remained stable (interstimulus interval = 60s). Usually, it was possible to induce several transient depressions of the uIPSPs or uIPSCs by repeating cycles ofthe stimulationprotocol followed by low frequency stimulations in the same cell pair (note the average values and SEM bars of Figure 1C). We termed the transient depression of the uIPSPs or uIPSCsas “firing induced suppression of inhibition” (FSI). Quantitatively, the FSI of the uIPSPs recorded in current clamp was not significantly different from the FSI of the uIPSCs recorded in voltage clamp ($p > 0.1$, Figure 1D). Therefore, data arising from both recording modes were pooled and will be presented as such in the next sections. Most of the presynaptic neurons displayed autaptic IPSCs (aIPSCs,see below). Interestingly, the stimulation protocol also induced FSI of theaIPSPs or aIPSCs in six out of thirty pairs that also showed FSI of the postsynaptic uIPSPs or uIPSCs, although this transient depression was mild(92.5 ± 1.8% of control, $p < 0.05$, data not shown).

Next we aimed to confirm that the recorded neurons in the SLM were NGFCs, since this layer of the hippocampus contains the soma of several other interneuron types (Vida et al., 1998; Klausberger, 2009;Capogna, 2011).Therefore, the recorded neurons were tested for the presence of theaIPSPoccurring as a depolarizing potential (current clamp mode) or an inward current (voltage clamp mode) immediately after an action potential or current, the autaptic response being predictive of anNGFC(Karayannis et al., 2010). Furthermore, the kinetics of the postsynaptic uIPSCs were analysed; when the

rise-time was > 3 ms and the decay time constant > 60 ms, the presynaptic neuron was considered asan NGFC based on our previous observations(Karayannis et al., 2010). Furthermore, all neurons were filled with biocytinfor subsequent analysisof the dendritic and axonal patterns. Based on these three criteria combined, we found that 29/34 presynaptic neurons displaying FSI were NGFCs, characterized by round somata, short, highly arborizing dendrites close to the soma and an axon which profusely arborized to cover the dendritic tree (Figure 2A).Furthermore, 5/34 wereother types of interneuronsincludingtwo putative perforant path-associated interneurons, identified by the axonal branches segregated within the hippocampal fissure, and three putative cholecystokinin (CCK)-expressing basket neurons, characterized by the flask-like shape of their soma. Furthermore, we successfully recovered substantial portions of the dendritic and axonal processes in 15 postsynaptic neurons showing FSI. Amongst them,12 cells were identified as NGFCs, twocells as putative perforant path-associated interneurons, and onecell was classified as a putative CCK-expressing basket cell. The NGFCs and few other interneurons of the SLM included in this study exhibited firing patterns and intrinsic electrophysiological responses(data not shown) consistent with previous reportse.g. (Elfant et al., 2008).

Initial experiments ruled out that FSI was simply due to a transient and unspecific change in the postsynaptic membrane conductance. Specifically,application of a hyperpolarizing current pulse (-150 pA, 350 ms) into the postsynaptic cell before and immediately after the stimulationprotocoldid not modify thecells' membrane input resistance (97.3 ± 1.2% of control after the train,$p > 0.05$, $n = 18$, data not shown). This suggests that achange in membrane conductance did not account for the decrease in the amplitude of the synaptic responses observed. Moreover, FSI was not affected by the application of a $GABA_B$ receptor antagonist (CGP35348, 50 µM, $p > 0.5$, $n = 4$, data

not shown). This indicates that, although presynaptic $GABA_B$ receptorstightly control axonalGABA release from NGFCs(Price et al., 2005; Price et al., 2008), $GABA_B$ receptor activation is not involved inFSI.

In summary,*in vivo*NGFCfiring during hippocampal theta rhythm induces a DSI-like event,we termed FSI. In the next experiments we sought to determine the mechanisms involved in this phenomenon.

What triggers FSI in the postsynaptic neuron?

FSI was initiated by the postsynaptic neuron firing, suggestingthat an active process occurring in the dendrites was likely tobe involved. According to this idea, AP back-propagation (bAP) should occur along the postsynaptic dendrites in order to trigger this event. To test this hypothesis, we visualized bAPs in 24 interneurons of the SLM by using single cell voltage imaging as described in the Methods (Figure 2A). We analyzed $\Delta F/F$ signals at various dendritic locations associated with a somatic AP evoked by intracellular current injection. The cells tested with this protocol included NGFCs (n = 9), but also other interneurons of the SLM such as putative perforant path associated and CCK-expressing basket cells (n = 15). We observed a $\Delta F/F$ signal with an AP shape at all dendritic locations and in all interneurons studied. Since the amount of dye distributed along the dendritic axis may vary, to quantify the signal we performed a calibration protocol of $\Delta F/F$ signals using injection of long-lasting hyperpolarizing current pulses into the soma as described in the Methods. The calibration procedure is shown in Figure 2B. Using this procedure, we observed robust bAPs along the dendrites of NGFCs and other hippocampal interneurons of the SLM without any significant decrement ($p > 0.5$, $n = 24$). A summary of the quantification of the bAP along the dendrites of all interneurons studied with VSDis shown in Figure 2C. Optically

recorded bAP events were always associated with somatic APs, and both signals were abolished by the application of tetrodotoxin (TTX, 1 µM, Figure 2D). Thus, APs back-propagated along the dendrites of NGFCs and other interneurons of the SLM, and this event is likely to initiate FSI.

In the next series of experiments, we tested the hypothesis that the postsynaptic bAPselicited an increase in the dendritic Ca^{2+} concentration. First, we injected the stimulation protocol to induce FSI, and then we applied subthreshold depolarizing current pulses (75 pA x 1ms) with the same temporal pattern of the *in vivo* action potentials. This protocol was unable to induce FSI in all cell pairs tested (97.4 ± 2.5% of control, p >0.5, n = 11, Figure 3), consistent with the voltage imaging data.Secondly, postsynaptic neurons were recorded with a solution containing the Ca^{2+}chelator BAPTA (10 mM). In these experiments, only pairs showing FSI immediately after the formation of whole-cell patch clamp recording were tested. Under this condition,FSI was progressively attenuated (FSI at the onset of the recording was 69.7± 4.6% and 86.7± 3.0% of control after 8 ± 2 min., p < 0.05, n = 4), consistent with the delayed action of BAPTA at the distal dendritic sites of the recorded interneurons. Thirdly, we investigated the source of dendritic Ca^{2+} leading to FSI. In this respect, we have tested the involvement of intracellular Ca^{2+}stores(Collin et al., 2005). Experimentally, we inserted ryanodine (200 µm)and U73122 (3 µm)intothe patch pipette recording from postsynaptic cellsto inhibit Ca^{2+} release from the endoplasmic reticulum and phospholipase C (PLC), an important component of the Ca^{2+}signaling cascade, respectively. However, the diffusion of these blockers in the postsynaptic cell did not alter FSI. On average, FSI was initially 83.5 ± 6.2% of baseline and 78.9 ± 7.4% after 18 min.of recording (p > 0.1, n = 3, not shown). This result rules out that the endoplasmic reticulum is a relevant source of Ca^{2+} for FSI induction. As a positive

control, we observed that the insertion of ryanodine (200 μm) and U73122 (3 μm) in the presynaptic cell gradually inhibited the uIPSCsin experiments lasting ~ 20 min. (not shown).

Alternatively, Ca^{2+}entry through dendritic L-type Ca^{2+} channels could trigger FSI, consistent with their involvement on short-term plasticity, but not on baseline GABAergic transmission(Jensen and Mody, 2001). In all neurons tested, bath applied nimodipine(10μm) inhibited FSI without affecting the size of uIPSCs evoked by low frequency of stimulation. On average, FSI was 70.9 ±6.0% of baseline and 96.7 ± 3.5% initially and after 20 min. of nimodipine application ($p < 0.01$, $n = 4$) (Figure 4).

Taken together, these results suggest that L-type Ca^{2+} channels, but not ryanodine-sensitive Ca^{2+} stores, are involved in FSI induction.

Next, to directly measure Ca^{2+} signals associated with the stimulation firing protocol, we performed Ca^{2+} imaging experiments of NGFC dendrites using the low-affinity indicator OG5N (0.5 mM) to minimize the physiological perturbation of the Ca^{2+} homeostasis. First, we measured the dendritic Ca^{2+}signal associated with a single AP (Figure 5A) and with a train of ten APs at 100 Hz (Figure 5B). As shown in the figure, the Ca^{2+} transient associated with the AP train had a slower decay time compared to that associated with a single AP. Then, we measured the Ca^{2+}signal associated with the stimulation protocol and compared it with the linear sum of a single AP response template. As expected from the previous series of experiments, the Ca^{2+} signal associated with the stimulation protocol was larger than that obtained by summation of template signals. Crucially, this supralinear Ca^{2+} summation,as quantified by the difference of the Ca^{2+} signalat the end and 10 s after the onset of the stimulation protocol, was significantly larger in the postsynaptic neurons showing FSI than in the postsynaptic cells that did not display FSI (Figure 5C, D, $n = 6$ each group, $p < 0.05$). In

order to estimate the change in dendritic free Ca^{2+} concentration associated with an action potential and with the stimulation protocol we performed a series of calibration experiments using both OG5N and MF2 in the pipette. Comparison of ΔF/F signals associated with three different stimulation protocols (5, 10 or 20APs at 100 Hz) gave a conversion factor of ~2.5 for OG5N (Figure 5E) indicating that ΔF/F=1% corresponded approximately to a free Ca^{2+} concentration change of 100 nM for this indicator, assuming a K_d = 25 μM for MF2 (Cueni et al., 2008). We conclude that a sustained elevation of free Ca^{2+} in the dendrites of the postsynaptic neuron (typically > 1 μM) is associated with the stimulation protocol that induces FSI. Such prolonged increase in dendritic Ca^{2+}could lead to the release of a chemical messenger.

What messenger(s) is responsible for FSI?

What messenger triggersFSI? The nNOSis expresses by several hippocampal interneurons including NGFCs (Price et al., 2005; Tricoire et al., 2010;Tricoire and Vitalis, 2012). Furthermore, the NO-sensitive guanylylcyclase (NO-sGC) receptor has been detected in the axon terminals and in the soma-dendritic compartment of various types of hippocampal interneurons (Szabadits et al., 2007). Both signals are highly enriched in the SLM of the hippocampus(Szabadits et al., 2007). Therefore, NO couldbe released from the dendrites of NGFCs and some other interneuron types of the SLM, diffuseretrogradely, and inhibit the release of GABA from other interneurons. We tested this hypothesis by studying the action ofthe nNOS inhibitor L-NAME (200 μM) on FSI. We first injected the stimulation protocolin a postsynaptic neuronto induce FSI (76.7 ± 2.5%, $p < 0.001$, $n = 11$). Next, we applied the nNOS inhibitor L-NAME (200 μM) for at least 10 minutes and the stimulation protocolwas repeated. Strikingly, we found thatL-NAME abolished FSI (95.1 ± 2.4%, $p < 0.001$,$n = 10/11$) (Figure 6). It is worth

noting that we found no significant effect of 200 μM L-NAME on spontaneous (s)IPSCs (in the presence of 3mM kynurenic acid to block sEPSCs, n = 3, data not shown). Both amplitude and inter-events distributions of sIPSCswere not significantly different in control and in the presence of L-NAME ($p > 0.1$ Kolmogorov-Smirnov test for each cell). This result suggests that the intracellular NO level is low under baseline conditions.Moreover, L-NAME did not affect the peak amplitude or the kinetics of single VSD-recorded bAP elicited 125 msafter 60 sstimulation firing (n = 10). The bAPpeak amplitude and the half width was not changed by L-NAME ($p > 0.1$, n = 10, not shown),further indicatingthat NO is released downstream of the APs back-propagating along the dendrites of the interneurons.

Further experiments confirmed the involvement of NO as a signal mediating FSI. Firstly, we investigated whether blocking the NO-sGC receptor, the main effector of NO, abolished FSI. Similar to the nNOS inhibitor, bath application of ODQ (10 μM),a NO-sGC receptor antagonist, applied for at least 10 minutes,blocked FSI that was successfully induced before the application of the drug in each cell tested (Figure 7) (FSI control was 71.1± 3.7% and during ODQ was 96.8± 2.3%,$p < 0.01$,n = 8). Secondly, the application of the NO precursor L-arginine (1 mM, n = 5) (Palmer et al., 1988)potentiatedFSI (FSI control was 73.1 ± 4.4% and during L-arginine was 62.4± 6.1%,$p < 0.05$,n = 5, not shown).Thirdly, the application of the NO donor SNP (200μM) occluded FSI, consistent with theidea that this agent would saturate NO receptors and with theaction of this drug on NO-mediated modulationof excitatory synaptic events (Makara et al., 2007).On average, FSI was 72.4 ± 5.6% before and 96.5 ± 6.3% in the presence of SNP, n = 6, $p < 0.05$, not shown). Fourthly, L-NAME blocked FSI in the presence of the cannabinoid receptor 1 (CB1) antagonist AM-251(not shown, FSI was 74.1 ± 6.1% in control, 77.9 ± 5.3% in the presence of AM-251, $p > 0.05$, and 97.4 ±

3.9% after addition of L-NAME, $p < 0.05$, $n = 3$). Finally, the likelihood of FSI detection was enhanced when synaptically-coupled pairs oftdTomato-labelled nNOS neurons were recorded in annNOS-Cre-tdTomatomouse line (Figure 8A-D). In these experiments 7 out of 9 cell pairs tested showed a robust FSI ($69.4 \pm 2.6\%$, $p < 0.001$) induced by the stimulation protocol.This frequency of occurrence of FSI was significantly higher than the probability of FSI occurrence in pairs recorded from control rats (78% versus 35% FSI detection, $p < 0.01$, chi square test)(Figure 8D). The FSI observed when recording from tdTomato-labelled nNOS neuronswas blocked by 200 μM L-NAME or 10 μM ODQ ($n = 3$, data not shown). Control analysis showed that the nNOS-CreER driver correctly labelled nNOS positive neurons. To this end, three tdTomato mice ($n = 3$) have been perfused, their brain fixed and tested for a specific antibody against nNOS. The great majority of tdTomato expressing hippocampal neurons from these mice were immunolabelled for nNOS(98 out of 104 of counted cells,Figure 8E, F).

Taken together, our data suggest that NO is the signalresponsible for FSI. It is likely that NOisreleased from the dendrites of NGFCs, diffusesretrogradely, binds to specific presynaptic receptors and inhibits the release of GABA from other NGFCs.

Physiological implications of FSI

To test the physiological role of FSI on single cell integration, we recorded putative unitary EPSPs in NGFCs evoked by the minimal stimulation of the SLM at gammafrequency in the presence of 5 μM gabazine and 50 μM CGP35348 to block synaptic inhibition. This stimulation evoked short-termEPSP facilitation followed by depression, as we have previously reported(Price et al., 2005). On note, the stimulation

protocol (*in vivo* firing pattern) did not evoke any significant change in the amplitude of these EPSPs, excluding a retrograde modulation of excitatory synapses (on average the EPSPs immediately after the firing protocol were 95.8 ± 7.0% of control, $p > 0.5$, $n = 3$, not shown).Next, we injected a train of EPSPs as synaptic conductance by using dynamic clamp (dEPSPs) in postsynaptic NGFCs (Figure 9).Since NGFCs have short dendrites and are biophysically compact, the somatic injection of unitary dEPSPs should represent a realistic representation of EPSPs evoked by stimulation of one or a few fibres present in the SLM, such as the perforant path from the entorhinal cortex. Coincident with dEPSPsinjection, an action potential in a presynaptic NGFC was also evoked, and this elicited a hyperpolarizinguIPSP in the postsynaptic NGFC. Next,the stimulation protocol (*in vivo* firing pattern) was applied to the postsynaptic NGFC, to induce FSI and transiently reduce the size of the uIPSP (69.4 ± 10.6% of control, $p < 0.05$, $n = 8$). We observed that when FSI occurred, the amplitude of the dEPSPs was significantly increased (Figure 9)($p < 0.05$ for the first threedEPSPsof the train,$n = 8$) compared to dEPSPs elicited in the presence ofcontrol synaptic inhibition before or after FSI. Remarkably, this effect affected several sequential dEPSPs, consistent with the long-lasting duration of NGFC-evoked uIPSPs(Tamas et al., 2003; Price et al., 2005). Thus, FSI transiently increased the size of the dEPSPs thereby promoting thetemporal/spatial integration of the uEPSPselicited by stimulation of perforant path/other excitatory fibres present in the SLM.

Discussion

The data suggest novel physiological roles for the rhythmic firing of hippocampal NGFCs during theta oscillationsand for the presence of NO in this interneuron type. We report thatNO acts as a transmitter, released by the dendrites and likely acting at

presynaptic site,to modulate the strength of local inhibitory circuits, an event we called FSI. We also show that FSI transiently modifies the strength of incoming excitatory postsynaptic potentials onto interneurons.

The FSI plastic event reported here resembles the classical DSI phenomenon consisting of postsynaptic depolarization-induced suppression of synaptic inhibition(Alger, 2012).However we triggered FSI by the injection of a firing sequence recorded *in vivo* during theta oscillations (Fuentealba et al., 2010)and replayed in the same cell type *in vitro*. In contrast, DSI is usually triggered by a prolonged steady depolarization of the postsynaptic neuron (Regehr et al., 2009). (cf. however,(Dubruc et al., 2013)). We used an*in vivo* firing sequence during theta oscillations because this rhythm is physiologicallyrelevant and it is clearly detected in the SLM(Buzsaki, 2002). Thefiring of NGFCs may have an important role in this rhythm (Capogna and Pearce, 2011). A firing sequence shorter than 60s (10-30s) produced less robust and reliable FSI (not shown). However, we have not systematically addressed the issue of the optimal firing duration needed to evoke NO release.

Since FSI is evoked by the firing of the postsynaptic neuron, the next step has been to test whether bAPswere present in these neurons. We studied this issue by recordingbAPs with voltage imaging at different dendritic sites (range: 20-120 μm from the soma). We found that bAPs were present in all interneurons of the SLM tested and was particularly robustin NGFCs. The bAPs were also detected in the dendrites after the injection of the *in vivo* firing used as stimulation protocol to induce FSI, suggesting a faithful propagation of the signal during physiologically-relevant firing. Previous data obtained by using Ca^{2+} imaging or dual dendritic and somatic patch clamp recording of hippocampal or cortical interneuronsreported significant attenuation of bAPs with distance from the soma because of the higher density of K^+ channels in distal dendrites

(Goldberg et al., 2003; Aponte et al., 2008; Topolnik et al., 2009; Hu et al., 2010; Evstratova et al., 2011).Other studies reported a more robust bAPs in dendrites of interneurons by using Ca^{2+}(Rozsa, 2004) or voltage imaging (Casale and McCormick, 2011). The notion that emerges from the present and previous studies is of neuron type-specific attenuation of bAPs along the dendrites of various interneuron types. Importantly, we observed that the L-type Ca^{2+} channels, but not Ca^{2+} stores, mediate FSI induction.Since baseline uIPSCs were not affected by a L-type Ca^{2+} channel antagonist,it is likely that Ca^{2+} influx through dendritic channels is involved in this effect. Thus, as for release of GABA at hippocampal synapses (Jensen and Mody, 2001), our data suggest that L-type Ca^{2+} channels are use-dependent. Our results are consistent with the finding that L-type Ca^{2+} channels,in addition to N-type Ca^{2+} channels, initiate DSI (Lenz et al., 1998). Interestingly, when we monitored dendritic Ca^{2+} levels during the stimulation protocol used to induce FSI we found an excellent correlation between the presence of FSI and supralinear Ca^{2+} signal. This result suggests that bAP-dependent rise of Ca^{2+} is required to trigger the release of retrograde signal(s) mediating FSI. The mechanisms underlying such differences in dendritic Ca^{2+} levels observed in our studyremain unknown. Several factors could be involved such as heterogeneous Ca^{2+} buffering properties, various Ca^{2+} extrusion rate or variable distribution of dendriticCa^{2+}channel type/concentration amongst different neuronsstudied.

Next, we identified NO as the signalmediating FSI. Our data are consistent with the idea that the prolonged physiological firing of the postsynaptic cell leads to Ca^{2+}-dependent release of NO from dendrites which activates presynaptic NO-sGC receptors which, in turn, depresses GABA release from axon terminals. Our pharmacological results clearly involved NO as a signal mediating FSI:the non-specific nNOS inhibitor L-NAME blocked FSI in virtually all cell pairs tested, the specific NO-sGCreceptor

blocker ODQ abolished FSI in all cell pairs tested, the NO precursor L-arginine tended to potentiate FSI, and pairs of Td-Tomato-nNOS expressing neurons displayed a significantly higher frequency of FSI occurrence compared to randomly recorded pairs. A dendritic release of NO is consistent withits gaseous nature that does not require vesicles for its release (Garthwaite, 2008). It is important to note that our data cannot firmly exclude a purely postsynaptic mechanism, although the kinetics of uIPSCs during FSI was indistinguishable from that of control uIPSCs, a result that makes a postsynaptic modulation of the $GABA_A$ receptorunlikely. Additional functional tests to investigate presynaptic *versus* postsynaptic mechanisms (such as the CV analysis of the synaptic responses) were precluded by the need of collecting tens of uIPSCs to perform this analysis. This would have requiredunrealistic long-lasting recordings due to the well-known requirement of low frequency stimulation to evoke stable NGFC-mediated events (Tamas et al., 2003; Price et al., 2005). Our results are consistent with data showing high expression of the NO-sGC receptor in the SLM,and with the detection of the molecular machinery for retrograde NO signalling, such as NOs in hippocampal interneurons (Szabadits *et al.*, 2007) in addition to CA1 pyramidal cells (Burette et al., 2002). Functionally, it has been reported that NO released from CA1 pyramidal cell retrogradelymediates DSI (Makara et al., 2007).However, this effect by NO was only observed after prior activation of the muscarinic acetylcholine receptor and it was triggered by the steady depolarization of the postsynaptic neuron(Makara et al., 2007).

Theevidence that NO is a retrograde signal released from postsynaptic GABAergic neurons totransiently depress synaptic inhibition is unprecedented to our knowledge. An endocannabinoid is the classical retrograde mediator of DSI including synaptic connections between hippocampal interneuron-principal cell (Ohno-Shosaku et al., 2001; Wilson and Nicoll, 2001), hippocampal radiatum CCK expressing

interneurons (Ali, 2007), and also mediates the self-induced hyperpolarization of low-threshold spiking dendrite-targeting cortical interneurons (Bacci et al., 2004).

What cell types of the hippocampal SLM are involved in FSI? The great majority of anatomically-identified recorded pairs exhibiting FSI were identified as NGFCs. This cell type expressesnNOS together with several other non-specific markersin the rodent hippocampus (Price et al., 2005; Fuentealba et al., 2010). Fate-mapping analysis shows that hippocampal NGFCs derived from the median ganglionic eminence express nNOS whereasNGFCs originatingin the caudal ganglionic eminence are nNOS negative (Tricoire et al., 2010; Tricoire and Vitalis, 2012). Our data demonstratea selective influence of nNOS expressing NGFCs on local synaptic activity. Moreover, a small percentage of pairs displaying FSI were likely to beperforant path-associated or CCK basket interneurons. This latterinterneuron typeis well known to express the CB_1 receptor (Katona et al., 2001; Nyiri et al., 2005), but we previously observed thatCCKfrequently co-localizes with nNOSina single cell PCR analysis of SLM interneurons (Price et al., 2005). We cannot exclude that other types of interneurons of SLM including Schaffer collateral associatedcells could also be involved in FSI, because of non-recovery of some of our recorded cells or incompletesampling.

It is important to note that FSI was detectable only in ~30-40% of all synaptically-coupled pairs recorded without any bias, and that this percentage rose to ~80% when only nNOS-expressing interneurons of the SLM were tested. This finding agrees with the observations that some,but not all,NGFCs express nNOS(Tricoire et al., 2010) and that only a third of nNOS expressing **c**ells also express NO-sGCreceptor (Szabadits et al., 2007).

What is the functional role of FSI in the hippocampal networks? The SLM is an area of integration containing several excitatory inputs and local but also distant inhibitory inputs (Soltesz and Jones, 1995; Capogna, 2011;Melzer et al., 2012). Feed-forward inhibition (Buzsaki, 1984; Pouille and Scanziani, 2001; Jarsky et al., 2005; Price et al., 2008)limits the temporal summation of EPSPs and generates a narrow 'window of excitability' during which action potentials can occur in the postsynaptic neuron. We observed here that NGFC-mediated slow IPSPs modify the size of unitary EPSPs evoked by the stimulation of fibres present in the SLM such as the perforant pathway. Crucially, this effect was transiently attenuated by coincident-occurring FSI. Furthermore, chains of interneurons are likely to coordinate the spatiotemporal organization of distinct but connected networks(Mizuseki et al., 2009; Chamberland and Topolnik, 2012).We speculate that FSI occurring in interneurons of the SLM transiently strengthens the rhythmic coordination between the entorhinal cortex and the CA1 area of the hippocampus.

References

Alger BE (2012) Endocannabinoids at the synapse a decade after the dies mirabilis (29 March 2001): what we still do not know. J Physiol 590:2203-2212.

Ali AB (2007) Presynaptic Inhibition of GABAA Receptor-Mediated Unitary IPSPs by Cannabinoid Receptors at Synapses Between CCK-Positive Interneurons in Rat Hippocampus. Journal of Neurophysiology 98:861-869.

Aponte Y, Bischofberger J, Jonas P (2008) Efficient Ca2+ buffering in fast-spiking basket cells of rat hippocampus. The Journal of Physiology 586:2061-2075.

Bacci A, Huguenard JR, Prince DA (2004) Long-lasting self-inhibition of neocortical interneurons mediated by endocannabinoids. Nature 431:312-316.

Baimbridge KG, Celio MR, Rogers JH (1992) Calcium-binding proteins in the nervous system. Trends Neurosci 15:303-308.

Burette A, Zabel U, Weinberg RJ, Schmidt HH, Valtschanoff JG (2002) Synaptic localization of nitric oxide synthase and soluble guanylyl cyclase in the hippocampus. J Neurosci 22:8961-8970.

Buzsaki G (1984) Feed-forward inhibition in the hippocampal formation. Prog Neurobiol 22:131-153.

Buzsaki G (2002) Theta oscillations in the hippocampus. Neuron 33:325-340.

Caillard O, Moreno H, Schwaller B, Llano I, Celio MR, Marty A (2000) Role of the calcium-binding protein parvalbumin in short-term synaptic plasticity. Proc Natl Acad Sci U S A 97:13372-13377.

Canepari M, Vogt KE (2008) Dendritic spike saturation of endogenous calcium buffer and induction of postsynaptic cerebellar LTP. PLoS One 3:e4011.

Canepari M, Vogt K, Zecevic D (2008) Combining voltage and calcium imaging from neuronal dendrites. Cell Mol Neurobiol 28:1079-1093.

Canepari M, Willadt S, Zecevic D, Vogt KE (2010) Imaging Inhibitory Synaptic Potentials Using Voltage Sensitive Dyes. Biophysical Journal 98:2032-2040.

Capogna M (2011) Neurogliaform cells and other interneurons of stratum lacunosum-moleculare gate entorhinal-hippocampal dialogue. J Physiol 589:1875-1883.

Capogna M, Pearce RA (2011) GABA A,slow: causes and consequences. Trends Neurosci 34:101-112.

Casale AE, McCormick DA (2011) Active Action Potential Propagation But Not Initiation in Thalamic Interneuron Dendrites. Journal of Neuroscience 31:18289-18302.

Cauli B, Tong XK, Rancillac A, Serluca N, Lambolez B, Rossier J, Hamel E (2004) Cortical GABA interneurons in neurovascular coupling: relays for subcortical vasoactive pathways. J Neurosci 24:8940-8949.

Chamberland S, Topolnik L (2012) Inhibitory control of hippocampal inhibitory neurons. Front Neurosci 6:165.

Collin T, Marty A, Llano I (2005) Presynaptic calcium stores and synaptic transmission. Curr Opin Neurobiol 15:275-281.

Colmers WF, Klapstein GJ, Fournier A, St-Pierre S, Treherne KA (1991) Presynaptic inhibition by neuropeptide Y in rat hippocampal slice in vitro is mediated by a Y2 receptor. Br J Pharmacol 102:41-44.

Cossart R, Dinocourt C, Hirsch JC, Merchan-Perez A, De Felipe J, Ben-Ari Y, Esclapez M, Bernard C (2001) Dendritic but not somatic GABAergic inhibition is decreased in experimental epilepsy. Nat Neurosci 4:52-62.

Cueni L, Canepari M, Lujan R, Emmenegger Y, Watanabe M, Bond CT, Franken P, Adelman JP, Luthi A (2008) T-type Ca2+ channels, SK2 channels and SERCAs gate sleep-related oscillations in thalamic dendrites. Nat Neurosci 11:683-692.

Dubruc F, Dupret D, Caillard O (2013) Self-tuning of inhibition by endocannabinoids shapes spike-time precision in CA1 pyramidal neurons. J Neurophysiol 110:1930-1944.

Elfant D, Pal BZ, Emptage N, Capogna M (2008) Specific inhibitory synapses shift the balance from feedforward to feedback inhibition of hippocampal CA1 pyramidal cells. Eur J Neurosci 27:104-113.

Evstratova A, Chamberland S, Topolnik L (2011) Cell type-specific and activity-dependent dynamics of action potential-evoked Ca2+ signals in dendrites of hippocampal inhibitory interneurons. The Journal of Physiology 589:1957-1977.

Freund TF, Ylinen A, Miettinen R, Pitkanen A, Lahtinen H, Baimbridge KG, Riekkinen PJ (1992) Pattern of neuronal death in the rat hippocampus after status epilepticus. Relationship to calcium binding protein content and ischemic vulnerability. Brain Res Bull 28:27-38.

Fuentealba P, Begum R, Capogna M, Jinno S, Marton LF, Csicsvari J, Thomson A, Somogyi P, Klausberger T (2008) Ivy cells: a population of nitric-oxide-producing, slow-spiking GABAergic neurons and their involvement in hippocampal network activity. Neuron 57:917-929.

Fuentealba P, Klausberger T, Karayannis T, Suen WY, Huck J, Tomioka R, Rockland K, Capogna M, Studer M, Morales M, Somogyi P (2010) Expression of COUP-TFII nuclear receptor in restricted GABAergic neuronal populations in the adult rat hippocampus. J Neurosci 30:1595-1609.

Garthwaite J (2008) Concepts of neural nitric oxide-mediated transmission. Eur J Neurosci 27:2783-2802.

Goldberg JH, Tamas G, Yuste R (2003) Ca2+ imaging of mouse neocortical interneurone dendrites: Ia-type K+ channels control action potential backpropagation. The Journal of Physiology 551:49-65.

Gulyas AI, Megias M, Emri Z, Freund TF (1999) Total number and ratio of excitatory and inhibitory synapses converging onto single interneurons of different types in the CA1 area of the rat hippocampus. J Neurosci 19:10082-10097.

Hu H, Martina M, Jonas P (2010) Dendritic mechanisms underlying rapid synaptic activation of fast-spiking hippocampal interneurons. Science 327:52-58.

Jarsky T, Roxin A, Kath WL, Spruston N (2005) Conditional dendritic spike propagation following distal synaptic activation of hippocampal CA1 pyramidal neurons. Nat Neurosci 8:1667-1676.

Jensen K, Mody I (2001) L-type Ca2+ channel-mediated short-term plasticity of GABAergic synapses. Nat Neurosci 4:975-976.

Karagiannis A, Gallopin T, David C, Battaglia D, Geoffroy H, Rossier J, Hillman EM, Staiger JF, Cauli B (2009) Classification of NPY-expressing neocortical interneurons. J Neurosci 29:3642-3659.

Karayannis T, Elfant D, Huerta-Ocampo I, Teki S, Scott RS, Rusakov DA, Jones MV, Capogna M (2010) Slow GABA transient and receptor desensitization shape synaptic responses evoked by hippocampal neurogliaform cells. J Neurosci 30:9898-9909.

Katona I, Rancz EA, Acsady L, Ledent C, Mackie K, Hajos N, Freund TF (2001) Distribution of CB1 cannabinoid receptors in the amygdala and their role in the control of GABAergic transmission. J Neurosci 21:9506-9518.

Klausberger T (2009) GABAergic interneurons targeting dendrites of pyramidal cells in the CA1 area of the hippocampus. Eur J Neurosci 30:947-957.

Klausberger T, Somogyi P (2008) Neuronal diversity and temporal dynamics: the unity of hippocampal circuit operations. Science 321:53-57.

Lenz RA, Wagner JJ, Alger BE (1998) N- and L-type calcium channel involvement in depolarization-induced suppression of inhibition in rat hippocampal CA1 cells. J Physiol 512 (Pt 1):61-73.

Llano I, Leresche N, Marty A (1991) Calcium entry increases the sensitivity of cerebellar Purkinje cells to applied GABA and decreases inhibitory synaptic currents. Neuron 6:565-574.

Maccaferri G, Lacaille JC (2003) Interneuron Diversity series: Hippocampal interneuron classifications--making things as simple as possible, not simpler. Trends Neurosci 26:564-571.

Makara JK, Katona I, Nyiri G, Nemeth B, Ledent C, Watanabe M, de Vente J, Freund TF, Hajos N (2007) Involvement of Nitric Oxide in Depolarization-Induced Suppression of Inhibition in Hippocampal Pyramidal Cells during Activation of Cholinergic Receptors. Journal of Neuroscience 27:10211-10222.

Melzer S, Michael M, Caputi A, Eliava M, Fuchs EC, Whittington MA, Monyer H (2012) Long-range-projecting GABAergic neurons modulate inhibition in hippocampus and entorhinal cortex. Science 335:1506-1510.

Mizuseki K, Sirota A, Pastalkova E, Buzsaki G (2009) Theta oscillations provide temporal windows for local circuit computation in the entorhinal-hippocampal loop. Neuron 64:267-280.

Nyiri G, Cserep C, Szabadits E, Mackie K, Freund TF (2005) CB1 cannabinoid receptors are enriched in the perisynaptic annulus and on preterminal segments of hippocampal GABAergic axons. Neuroscience 136:811-822.

Ohno-Shosaku T, Maejima T, Kano M (2001) Endogenous cannabinoids mediate retrograde signals from depolarized postsynaptic neurons to presynaptic terminals. Neuron 29:729-738.

Palmer RM, Ashton DS, Moncada S (1988) Vascular endothelial cells synthesize nitric oxide from L-arginine. Nature 333:664-666.

Pitler TA, Alger BE (1992) Postsynaptic spike firing reduces synaptic GABAA responses in hippocampal pyramidal cells. J Neurosci 12:4122-4132.

Pouille F, Scanziani M (2001) Enforcement of temporal fidelity in pyramidal cells by somatic feed-forward inhibition. Science 293:1159-1163.

Price CJ, Scott R, Rusakov DA, Capogna M (2008) GABA(B) receptor modulation of feedforward inhibition through hippocampal neurogliaform cells. J Neurosci 28:6974-6982.

Price CJ, Cauli B, Kovacs ER, Kulik A, Lambolez B, Shigemoto R, Capogna M (2005) Neurogliaform neurons form a novel inhibitory network in the hippocampal CA1 area. J Neurosci 25:6775-6786.

Regehr WG, Carey MR, Best AR (2009) Activity-Dependent Regulation of Synapses by Retrograde Messengers. Neuron 63:154-170.

Rozsa B (2004) Distance-Dependent Scaling of Calcium Transients Evoked by Backpropagating Spikes and Synaptic Activity in Dendrites of Hippocampal Interneurons. Journal of Neuroscience 24:661-670.

Soltesz I, Jones RS (1995) The direct perforant path input to CA1: excitatory or inhibitory? Hippocampus 5:101-103.

Szabadits E, Cserep C, Ludanyi A, Katona I, Gracia-Llanes J, Freund TF, Nyiri G (2007) Hippocampal GABAergic synapses possess the molecular machinery for retrograde nitric oxide signaling. J Neurosci 27:8101-8111.

Tamas G, Lorincz A, Simon A, Szabadics J (2003) Identified sources and targets of slow inhibition in the neocortex. Science 299:1902-1905.

Taniguchi H, He M, Wu P, Kim S, Paik R, Sugino K, Kvitsiani D, Fu Y, Lu J, Lin Y, Miyoshi G, Shima Y, Fishell G, Nelson SB, Huang ZJ (2011) A resource of Cre driver lines for genetic targeting of GABAergic neurons in cerebral cortex. Neuron 71:995-1013.

Topolnik L, Chamberland S, Pelletier JG, Ran I, Lacaille JC (2009) Activity-dependent compartmentalized regulation of dendritic Ca2+ signaling in hippocampal interneurons. J Neurosci 29:4658-4663.

Tricoire L, Vitalis T (2012) Neuronal nitric oxide synthase expressing neurons: a journey from birth to neuronal circuits. Front Neural Circuits 6:82.

Tricoire L, Pelkey KA, Daw MI, Sousa VH, Miyoshi G, Jeffries B, Cauli B, Fishell G, McBain CJ (2010) Common origins of hippocampal Ivy and nitric oxide synthase expressing neurogliaform cells. J Neurosci 30:2165-2176.

Vetter P, Roth A, Hausser M (2001) Propagation of action potentials in dendrites depends on dendritic morphology. J Neurophysiol 85:926-937.

Vida I, Halasy K, Szinyei C, Somogyi P, Buhl EH (1998) Unitary IPSPs evoked by interneurons at the stratum radiatum-stratum lacunosum-moleculare border in the CA1 area of the rat hippocampus in vitro. J Physiol 506 (Pt 3):755-773.

Wilson RI, Nicoll RA (2001) Endogenous cannabinoids mediate retrograde signalling at hippocampal synapses. Nature 410:588-592.

Figure Legends

Figure 1. NGFC *in vivo*firing pattern induces a transient suppression of synaptic inhibition (FSI). A, NGFC paired recording*in vitro*, current clamp mode, presynaptic action potentials (PRE, black traces) evoked depolarizing uIPSPs in a postsynaptic cell recorded with an electrode filled with 84 mMCl^- solution (POST, left dark blue traces superimposed recorded 120 s or 60 s before the stimulation protocol). Injection of firingrecorded *in vivo*from an NGFC for 60 s (stimulation protocol) in the postsynaptic NGFC recorded *in vitro* induced a transient decrease of the amplitude of the uIPSP (POST, middle trace), that returned to the baseline level 60 s and 120 s after the end of the stimulation protocol (right traces superimposed). **B,** NGFC paired recording, voltage clamp mode, presynaptic action currents (PRE, black traces) evoked inward uIPSCs in a postsynaptic cell recorded with an electrode filled with 84 mMCl^- solution (POST, left light blue traces superimposedrecorded 120 s or 60 s before the stimulation protocol). Injection of *in vivo*NGFC firing for 60 s (stimulation protocol) in the postsynaptic NGFC induced a transient decrease of the amplitude of the uIPSC (middle trace), that returned to the baseline level 60 s and 120 s after the end of the stimulation protocol (right traces superimposed). Inset, scaled traces show no changes in the kinetics of the uIPSCs before and during FSI.**C,**mean uIPSP (CC, current clamp) or uIPSC (VC, voltage clamp) peak amplitude before and after the stimulation protocol (repeated sequentially three times) for the cell pairs shown in A and B; error bars are SEM.**D**, summary of normalized peak amplitudes of uIPSPs (CC, current clamp) or uIPSCs (VC, voltage clamp) before and after the stimulation protocol in all pairs showing FSI, error bars are SEM ($p < 0.001$, $n = 23$ for CC data, $n = 11$ for VC data). In the graphs of panels **C** and **D**of this and subsequent figures, 0 s indicates mean uIPSP or uIPSC amplitude detected 125 or 250 ms after the end of the stimulus protocol.

Figure 2.bAP along the dendrites of NGFCs or other interneurons of the SLM. A, Image of an NGFC (after biocytin-streptoavidin-Cy3reaction) showing characteristic stellate dendrites (top picture, objective x20). This neuron was loaded with JPW-1114 and voltage imaging was performed from dendritic sites included in the red box; in particular, ΔF/F signals at the sites indicated (1-4, bottom picture, 4x4 pixels) were analyzed. **B**, Left, A depolarizing current pulse (800 pA, 3 ms) induced a somatic action potential (AP) recorded in current clamp (green trace) and the corresponding ΔF/F signals from the site 1-4 in A isillustrated. The red vertical bar denotes the AP peak recorded from the soma.**B**, Middle traces, fractional changes of voltage fluorescence (ΔF/F) in response to a ~ 10 mV membrane potentialhyperpolarization lasting 350 ms (average of 9 traces) injected into the soma and recorded from sites 1-4 of the dendrites; somatic current clamp recording is illustrated on the top. **B**, Right traces, ΔF/Fof the bAPs peak amplitude calibrated with the corresponding ΔF/Finduced by the hyperpolarizing current pulse recorded from regions 1-4 of the dendrites. **C**, group data of bAP peak amplitude recorded at different dendritic sites normalized to the bAP amplitude recorded at 20-30 μm (shortest distance) from the soma. Note that bAPs occurs in NGFCs and in other interneurons of the SLM (non-NGFC) without any significant decrement (bAP peak amplitude detected at dendrites >70 μm or ~20 μm away from the soma was not significantly different,$p > 0.5$, $n = 24$). **D,** Top trace, effect of 1μM TTX on an AP recorded in current clamp evoked by a depolarizing current pulse (800 pA x 3 ms, top traces). Bottom trace, effect of 1μM TTX on ΔF/F bAP recorded from a dendrite of an NGFC. Blue traces, control; Red traces, TTX. Note that TTX blocks the ΔF/F of the bAP, whereas it spares ΔF/F of the subthreshold depolarization evoked by the somatic subthreshold depolarizing pulse.

Figure 3. Stimulation protocol of weak subthreshold depolarizing current pulses does not elicit FSI.A, stimulation protocol (60 s, blue) applied to a postsynaptic NGFC (POST) elicited FSI of uIPSC peak amplitude (blue middle trace) recorded with an electrode filled with 84 mMCl^- solution and evoked by presynaptic action currents (PRE, black traces). In contrast, subsequent injection of weak subthreshold depolarizing current pulses (75 pA x 1 ms) (red) did not evoke FSI (red middle trace). Left and right traces show uIPSCs before and after FSI. **B**, mean uIPSCs peak amplitude before and after firing or subthreshold stimulation protocol for the data shown in A (dark symbols denote values immediately after stimulation protocol). **C**, normalized data (mean and SEM) for all cell pairs studied with this protocol (FSI controlwas 76.8 ± 2.7% and97.4 ± 2.5% with subthreshold pulses, n = 11).

Figure 4.The L-type Ca^{2+} blocker nimodipine inhibits FSI

A, Presynaptic action currents (PRE, black traces) evoked inward uIPSCs in a postsynaptic NGFC recorded with an electrode filled with 84 mMCl^- solution (POST, blue traces). Injection of the stimulation protocol in the postsynaptic cell induced a transient depression of the uIPSC amplitude (middle blue trace), that returned to control level 60 s after the end of the stimulation protocol (right blue trace). Application of the L-type Ca^{2+} channel blocker nimodipine (10 μM inhibited FSI (red traces). **B**, quantification of the uIPSC peak amplitude that occurred before or during the bath application of nimodipine for the data shown in A (dark symbols denote values immediately after stimulation protocol). **C**, normalized data (mean and SEM) for all uIPSCs studied with this protocol (FSI control was 70.9 ± 6.0% and 96.7 ± 3.5% with nimodipine, $p < 0.01$,n = 4).

Figure 5. Sustained elevation of Ca^{2+} in the dendrites of postsynaptic interneurons triggers FSI.

A, ΔF/F Ca^{2+} signal from anNGFCwith FSI (A1) or without FSI (A2) filled with OG5N (blue trace) associated with an AP (green trace, single trial). **B**, Same as A (in the same neurons) but for a train of ten APs at 100 Hz (single trial); note the increased decay time compared to the calcium signal associated with single AP; the red trace is the summation of 10 template ΔF/F Ca^{2+} signals associated with the single AP (note the faster decay time). **C,** ΔF/F Ca^{2+} signals (blue traces) associated with the stimulation protocol (green traces, single trial) from the dendrites of two NGFC cells, one exhibiting FSI (C1) and the other not showing FSI (C2); the red traces are again the linear summation of single AP template ΔF/F Ca^{2+} signals; note the larger supralinear summation of ΔF/F Ca^{2+} signals in the cell exhibiting FSI. **D**, Columns and error bars are the mean and the SEM of the difference of ΔF/F dendritic Ca^{2+} signal occurring 60 s and 10 s after the onset of the stimulation protocolsin postsynaptic neurons with FSI (blue column) and in cells without FSI (red column); this value in the two populations of neurons was significantly different ($n = 6$, $p < 0.05$). **E**, calibration of OG5N ΔF/F Ca^{2+} signal in terms of MF2 ΔF/F Ca^{2+} signal: plot of OG5N ΔF/F peak vs MF2 ΔF/F peak associated with different protocols (spade, 5 APs at 100 Hz; square, 10 APs at 100 Hz; triangle, 20 APs at 100 Hz, $n = 6$) in the same cells. The linear fit gives a conversion factor of 2.5; given that 1% for MF2 corresponds to ~250 nM, 1% for OG5N corresponds to ~100 nM.

Figure 6. The nNOS inhibitor L-NAME blocks FSI

A, Presynaptic APs (PRE, black traces) elicited depolarizing uIPSPs (control, left traces superimposed) recorded with an electrode filled with 84 mMCl^- solution showing FSI immediately after stimulation protocol applied to a postsynaptic NGFC (control, blue middle trace). The uIPSP recovered 60 s after the stimulation protocol (blue trace, right). Application of the nNOS inhibitor L-NAME (200μM) blocked FSI (red traces). **B**, quantification of the uIPSP peak amplitude that occurred before or after the stimulation protocol (dark symbols) in control and in the presence of L-NAME for the data shown in A. **C**, normalized data (mean and SEM, shaded areas) for all uIPSPs or uIPSCs studied with this protocol (FSI control was 76.6 ± 2.5%and 95.1 ± 2.4%with L-NAME, $p < 0.001$, $n = 10$).

Figure 7. The NO receptor antagonist ODQ blocks FSI

A, Presynaptic action currents (PRE, black traces) evoked inward uIPSCs in a postsynaptic NGFC recorded with an electrode filled with 84 mMCl^- solution (POST, blue traces). Injection of the stimulation protocol in the postsynaptic cell induced a transient depression of the uIPSC amplitude (middle blue trace), that returned to control level 60 s after the end of the stimulation protocol (right blue trace). Application of the NO receptor antagonist ODQ (10 μM) blocked FSI (red traces). **B**, quantification of the uIPSCpeak amplitude that occurred before or in the presence of ODQ for the data shown in A (dark symbols denote values immediately after stimulation protocol). **C**, normalized data (mean and SEM) for all uIPSPs or uIPSCs studied with this protocol (FSI control was 71.1 ± 3.7% and 96.8 ± 2.3% with ODQ, $p < 0.01$,$n = 8$).

Figure 8. FSI occurs frequently in pairs of neurons expressingnNOS-Cre-tdTomato

A, NGFC paired recording, voltage clamp mode, a presynaptic action current (PRE, black trace) evoked an inward uIPSC in a postsynaptic NGFC recorded with an electrode filled with 84 mMCl^- solution (POST, red traces superimposed). Injection of the stimulation protocol in the postsynaptic cell induced a transient depression of the uIPSC amplitude (middle trace), that returned to control level 60 s and 120 s after the stimulation protocol (right traces superimposed). **B,**uIPSC mean peak amplitude before and after the stimulation protocol for the data shown in A. **C**, summary of mean and SEM peak amplitudes of uIPSCs before and after the stimulation protocol in all pairs recorded (FSI = 69.4 ± 2.6%, $p < 0.001$, $n = 7$). **D**, bar graphs that the probability to observe FSI was significantly higher when pairs of tdTomato neurons were recorded compared to pairs recorded in wild type rats (78% versus 35% FSI detection, $p < 0.01$, chi square test). **E**, Examples of two tdTomato expressing neurons of the hippocampal SLM (left), also immunopositive for nNOS(middle); a merged picture is shown on the right. AnnNOSimmunopositive cell not expressing tdTomato is also visible. **F**, summary data, 98 out of 104 tdTomato expressing neurons also expressed nNOS.

Figure 9. FSI transiently modulates EPSPs impinging onto NGFCs

A, An EPSP train was injected as synaptic conductance using dynamic clamp (POST, dEPSPs, blue trace, - 60 s) in a postsynaptic NGFC while an action potential in a presynaptic NGFC (PRE, black trace) elicited a coincident uIPSP. Application of the stimulation protocol in the postsynaptic cell evoked a transient, smaller uIPSP (FSI). As a result, a significant enhanced depolarization level was reached by several dEPSPs of the train (red trace), the depolarization level of the EPSPs returned to the baseline 60 s after FSI (green trace, 60 s). **B**, **C**, normalized values of the dEPSPs amplitude during FSI (red bars) or 60 s after FSI (recovery, green bars) versus before FSI (blue

histograms), for the events shown above (B) or for all recorded cell pairs (C). In the presence of FSI, the first three dEPSPs had significantly larger amplitude than before FSI ($p < 0.05$, $n = 8$).

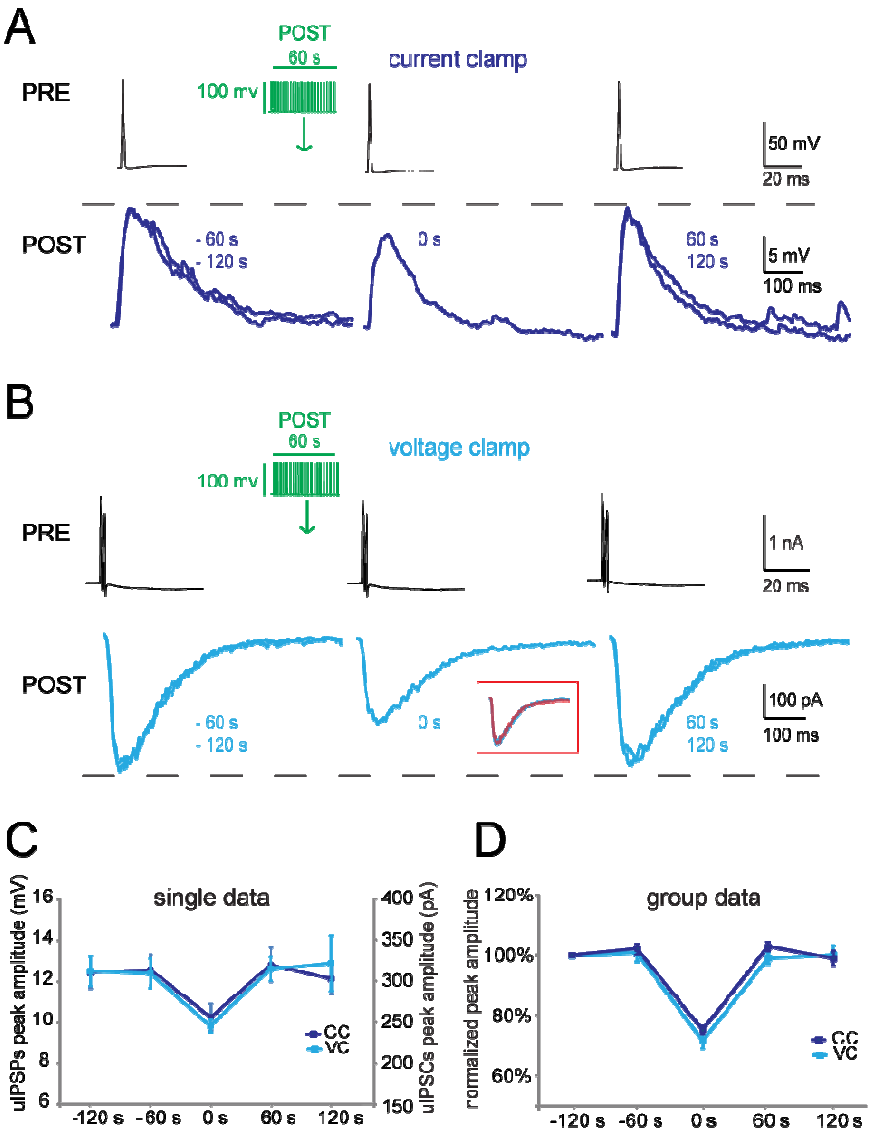

A
POST
60 s
current clamp
PRE
100 mv
50 mV
20 ms
POST
- 60 s
- 120 s
0 s
60 s
120 s
5 mV
100 ms
B
POST
60 s
voltage clamp
100 mv
PRE
1 nA
20 ms
POST
- 60 s
- 120 s
0 s
60 s
120 s
100 pA
100 ms
C
single data
uIPSPs peak amplitude (mV)
uIPSCs peak amplitude (pA)
CC
VC
-120 s
-60 s
0 s
60 s
120 s
D
group data
normalized peak amplitude
120%
100%
80%
60%
CC
VC
-120 s
-60 s
0 s
60 s
120 s

Figure 1

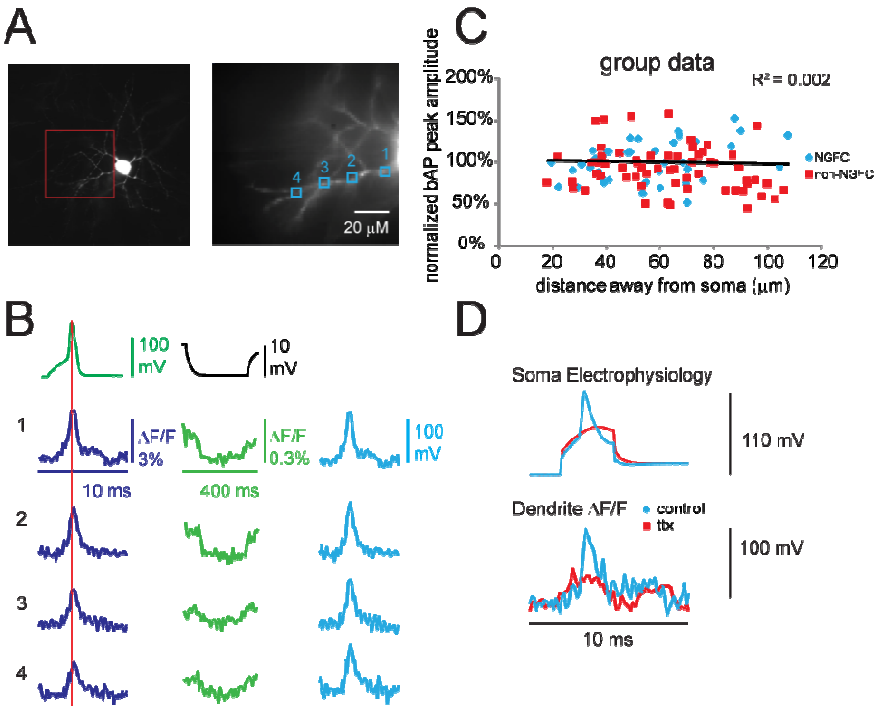

A
20 μM
4
3
2
1
B
100 mV
10 mV
1
ΔF/F 3%
ΔF/F 0.3%
100 mV
10 ms
400 ms
2
3
4
C
group data
R² = 0.002
normalized bAP peak amplitude
200%
150%
100%
50%
0%
0
20
40
60
80
100
120
distance away from soma (μm)
NGFC
non-NGFC
D
Soma Electrophysiology
110 mV
Dendrite ΔF/F
control
tbx
100 mV
10 ms

Figure 2

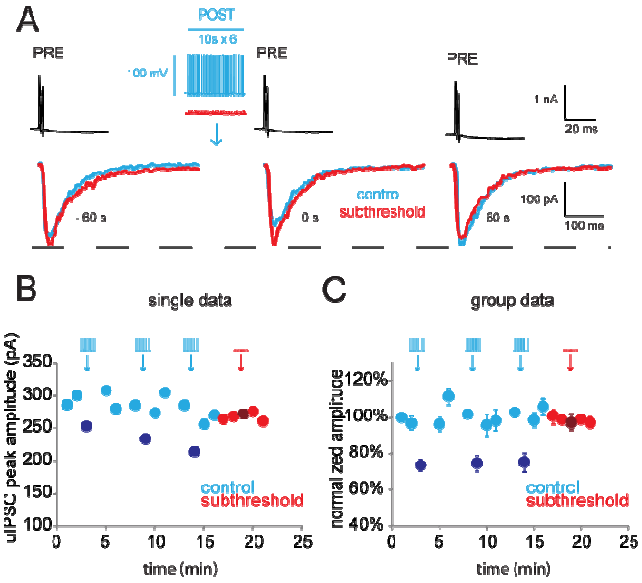

A
POST
10s x 6
PRE
PRE
PRE
1 nA
20 ms
0 s
control
subthreshold
50 s
100 pA
100 ms
B
single data
uIPSC peak amplitude (pA)
350
300
250
200
150
100
0
5
10
15
20
25
time (min)
control
subthreshold
C
group data
normal zed amplitude
120%
100%
80%
60%
40%
0
5
10
15
20
25
time (min)
control
subthreshold

Figure 3

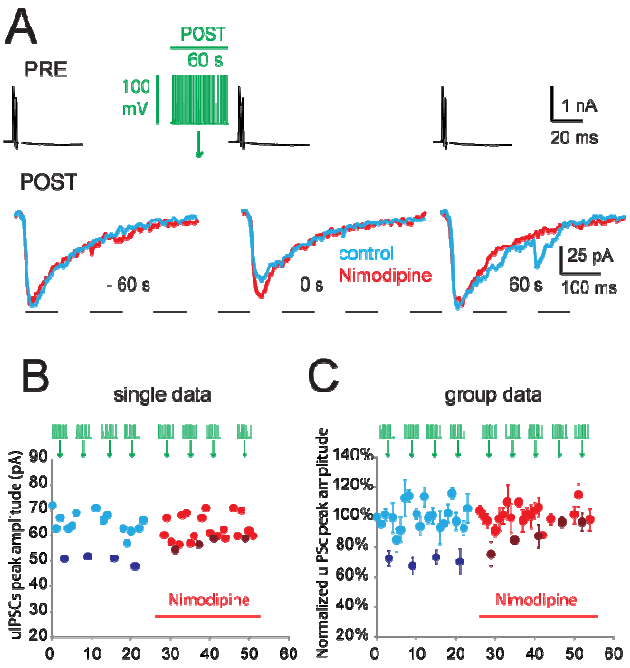

A
PRE
POST
60 s
100 mV
1 nA
20 ms
POST
- 60 s
0 s
control
Nimodipine
60 s
25 pA
100 ms
B
single data
uIPSCs peak amplitude (pA)
Nimodipine
C
group data
Normalized u PSC peak amplitude
Nimodipine

Figure 4

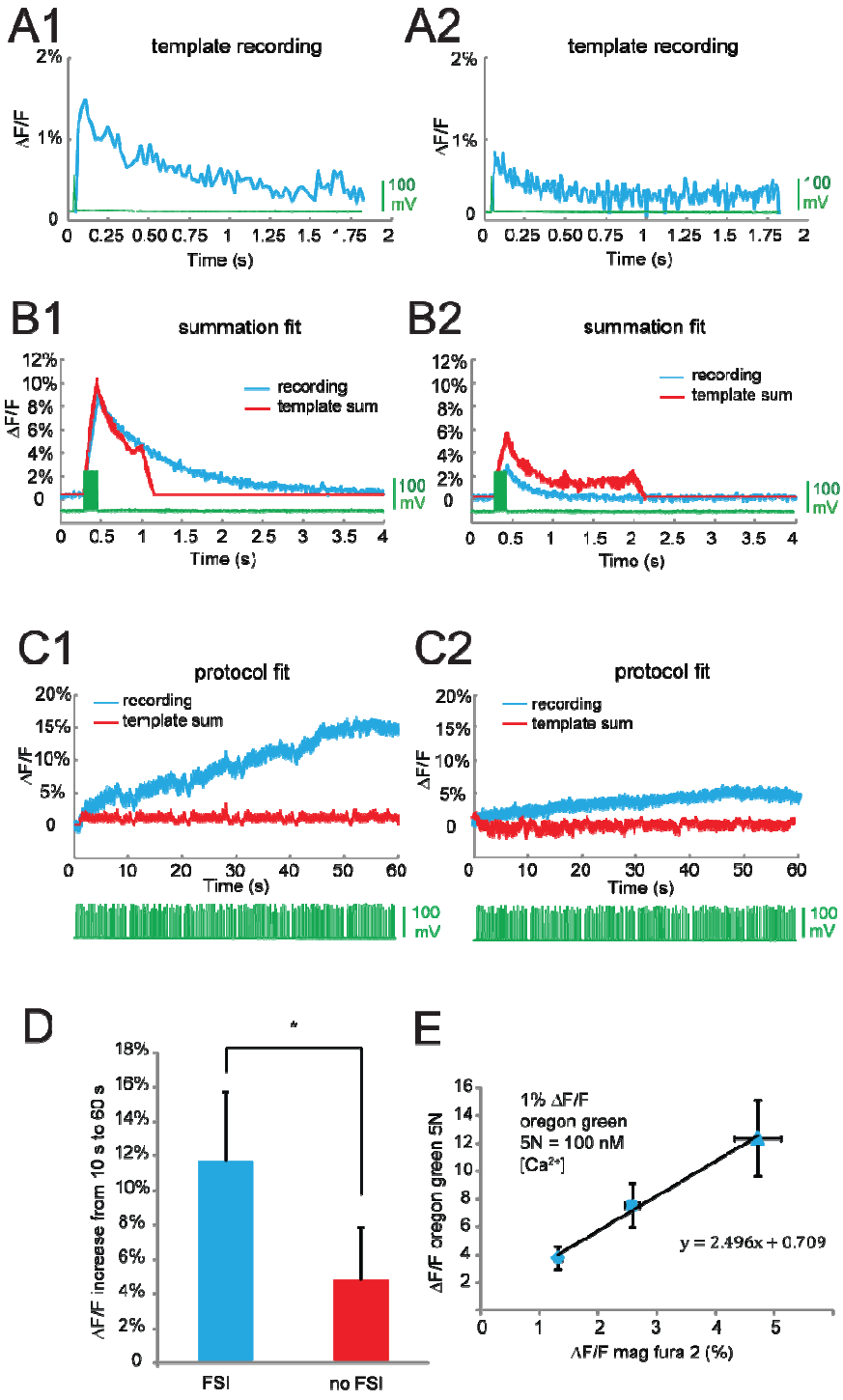

A1
template recording
2%
1%
0
ΔF/F
100 mV
0 0.25 0.50 0.75 1 1.25 1.5 1.75 2
Time (s)
A2
template recording
2%
1%
0
ΔF/F
100 mV
0 0.25 0.50 0.75 1 1.25 1.5 1.75 2
Time (s)
B1
summation fit
recording
template sum
12%
10%
8%
6%
4%
2%
0
ΔF/F
100 mV
0 0.5 1 1.5 2 2.5 3 3.5 4
Time (s)
B2
summation fit
recording
template sum
12%
10%
8%
6%
4%
2%
0
100 mV
0 0.5 1 1.5 2 2.5 3 3.5 4
Time (s)
C1
protocol fit
recording
template sum
20%
15%
10%
5%
0
ΔF/F
0 10 20 30 40 50 60
Time (s)
100 mV
C2
protocol fit
recording
template sum
20%
15%
10%
5%
0
ΔF/F
0 10 20 30 40 50 60
Time (s)
100 mV
D
*
18%
16%
14%
12%
10%
8%
6%
4%
2%
0
ΔF/F increase from 10 s to 60 s
FSI
no FSI
E
1% ΔF/F
oregon green
5N = 100 nM
[Ca2+]
y = 2.496x + 0.709
16
14
12
10
8
6
4
2
0
ΔF/F oregon green 5N
0 1 2 3 4 5
ΔF/F mag fura 2 (%)

Figure 5

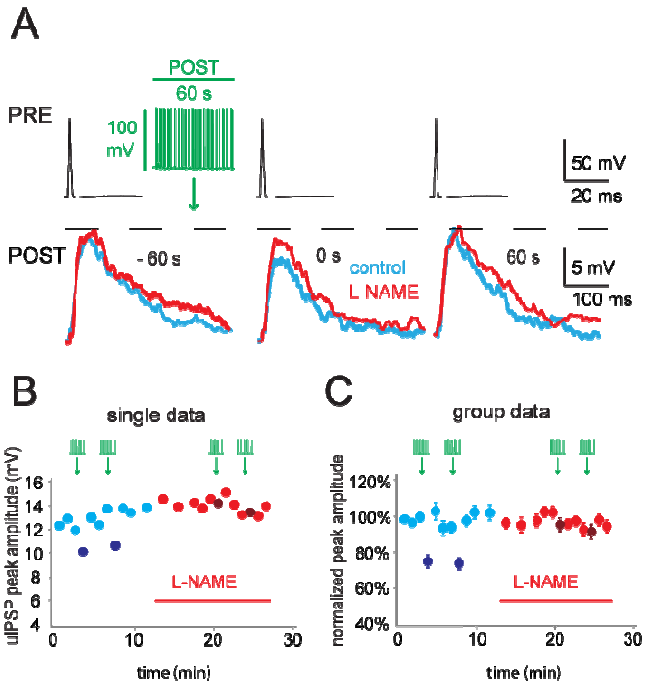

A
POST
60 s
PRE
100
mV
50 mV
20 ms
POST
-60 s
0 s
control
L NAME
60 s
5 mV
100 ms
B
single data
uIPSP peak amplitude (mV)
16
14
12
10
8
6
4
L-NAME
0
10
20
30
time (min)
C
group data
normalized peak amplitude
120%
100%
80%
60%
40%
L-NAME
0
10
20
30
time (min)

Figure 6

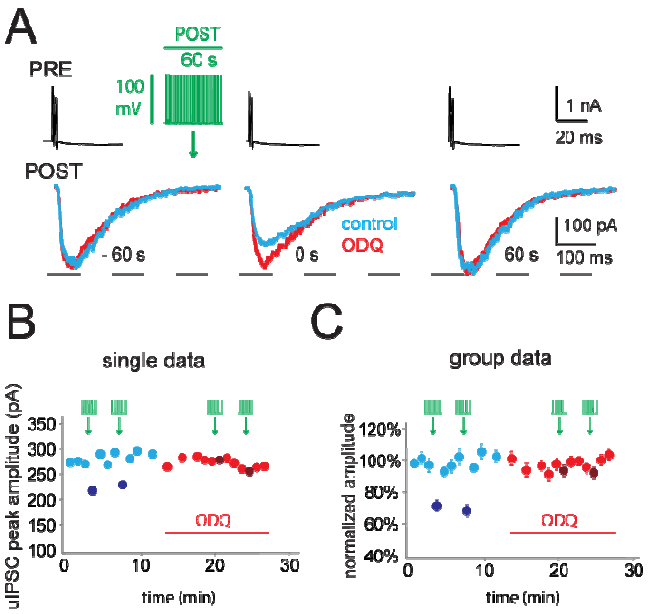

A
POST
60 s
PRE
100
mV
1 nA
20 ms
POST
- 60 s
0 s
control
ODQ
100 pA
100 ms
60 s
B
single data
C
group data
IPSC peak amplitude (pA)
350
300
250
200
150
100
ODQ
0
10
20
30
time (min)
normalized amplitude
120%
100%
80%
60%
40%
ODQ
0
10
20
30
time (min)

Figure 7

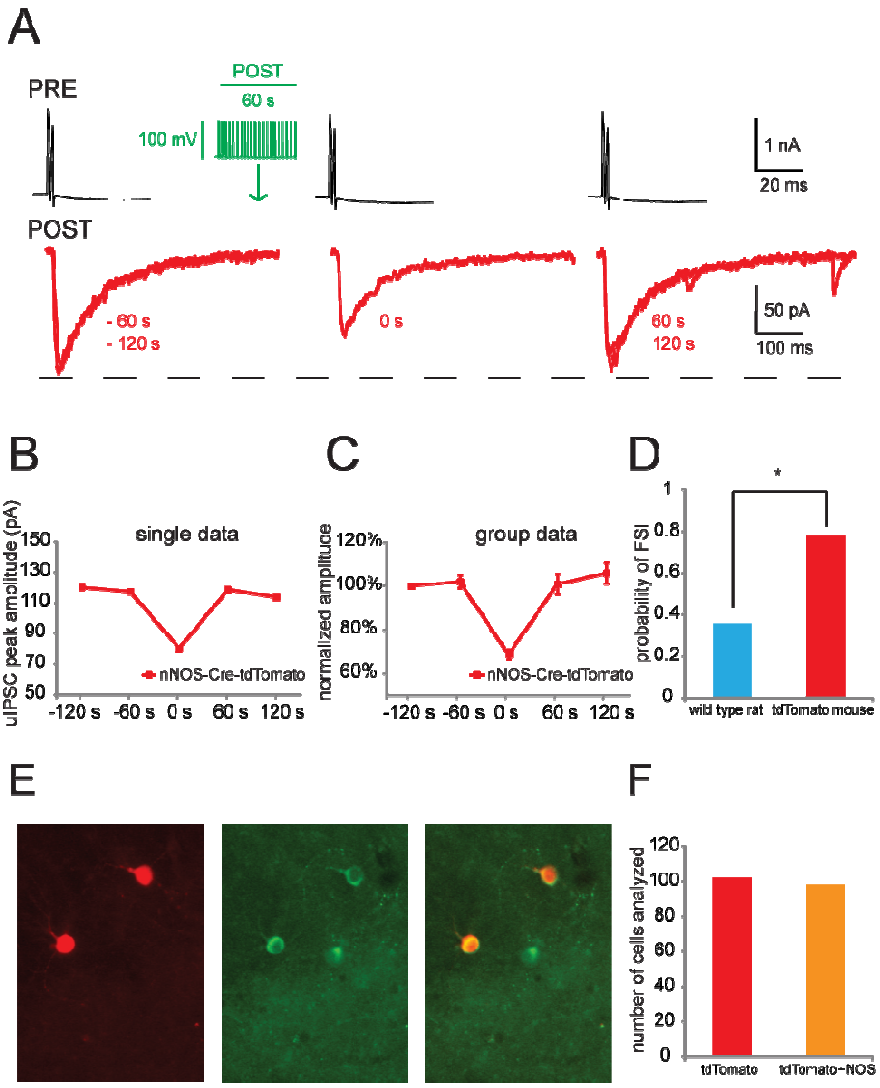

A
PRE
POST
60 s
100 mV
1 nA
20 ms
POST
- 60 s
- 120 s
0 s
60 s
120 s
50 pA
100 ms
B
single data
uIPSC peak amplitude (pA)
150
130
110
90
70
50
nNOS-Cre-tdTomato
-120 s -60 s 0 s 60 s 120 s
C
group data
normalized amplitude
120%
100%
80%
60%
nNOS-Cre-tdTomato
-120 s -60 s 0 s 60 s 120 s
D
*
probability of FSI
1
0.8
0.6
0.4
0.2
0
wild type rat
tdTomato mouse
E
F
number of cells analyzed
120
100
80
60
40
20
0
tdTomato
tdTomato-nNOS

Figure 8

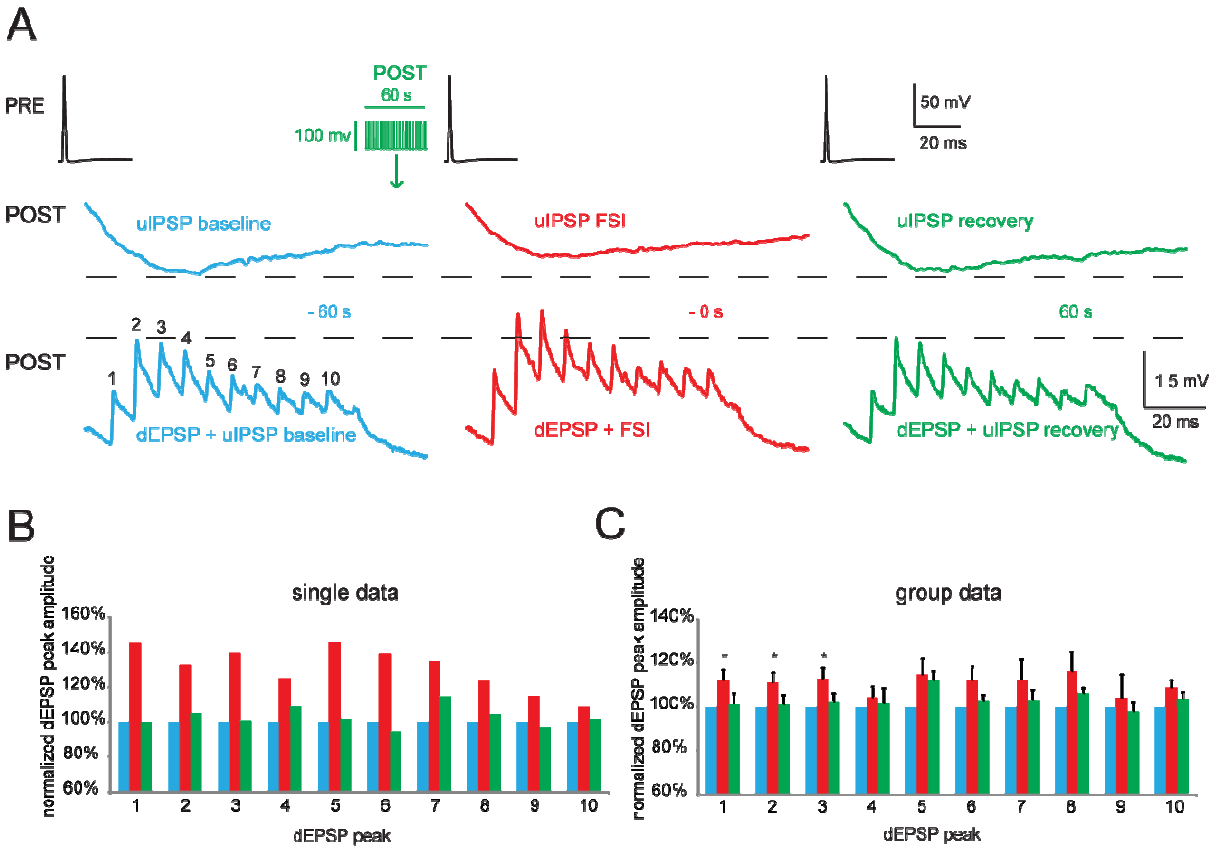

A
PRE
POST
60 s
100 mv
50 mV
20 ms
POST
uIPSP baseline
uIPSP FSI
uIPSP recovery
- 60 s
- 0 s
60 s
POST
1
2
3
4
5
6
7
8
9
10
dEPSP + uIPSP baseline
dEPSP + FSI
dEPSP + uIPSP recovery
1.5 mV
20 ms
B
single data
normalized dEPSP peak amplitude
160%
140%
120%
100%
80%
60%
1
2
3
4
5
6
7
8
9
10
dEPSP peak
C
group data
normalized dEPSP peak amplitude
140%
120%
100%
80%
60%
1
2
3
4
5
6
7
8
9
10
dEPSP peak

Figure 9